Strontium fluorapatite (S-FAP) nano-grained laser ceramics

Hiroaki Furuse [a]*, Yuki Mochizuki [b], Daichi Kato [b], Koji Morita [a], Byung-Nam Kim [a], and Tohru S. Suzuki [a]

[a] National Institute for Materials Science, 1-2-1 Sengen, Tsukuba, Ibaraki 305-047, Japan

[b] Kitami Institute of Technology, 165 Koen-cho, Kitami, Hokkaido 090-8507, Japan.

*Corresponding author E-mail: FURUSE.Hiroaki@nims.go.jp

Abstract:

The use of large-sized, highly transparent polycrystalline strontium fluorapatite (S-FAP) ceramics could be a breakthrough in the high-power laser field due to its excellent laser gain properties. However, its hexagonal crystal structure makes it difficult to obtain laser quality in polycrystalline ceramics owing to birefringence. In this study, fully densified transparent Nd- and Yb-doped S-FAP ceramics with an average grain size of ~100 nm can successfully be fabricated via liquid-phase nano-powder synthesis followed by spark plasma sintering, thereby achieving laser oscillation of the Nd:S-FAP ceramics for the first time. Furthermore, we elucidated the discrepancy in the emission properties between single-crystal and ceramics with randomly oriented crystal grains. We believe that these findings can provide important insights into the design and development for efficient non-cubic ceramic laser systems.

Keywords:

ceramics, optical materials, fluorapatite, spark plasma sintering, ultrafine grained microstructure

Ytterbium doped strontium fluorapatite (S-FAP: $Sr_{10}(PO_4)_6F_2$) single crystal has a larger stimulated emission-cross section than the typical yttrium-aluminum-garnet (YAG) laser material; hence, it is well known as high-average-power (i.e. high-pulse-energy and high-repetition-rate) laser host material. Particularly, a laser output of 60 J and 10 Hz was achieved with Yb:S-FAP single crystal in the early 2000s [1,2]. Recently, transparent Yb:YAG ceramics with high optical quality, which is comparable to those of single crystals, have been considered as representative high average power laser materials for 1 kW-class laser output [3,4]. Such high average power lasers with high pulse energy have potential applications in a wide range of fields, including laser processing, high-intensity laser physics, and medical applications.

The advantages of transparent ceramic technology for high-power laser output include the enlargeable size dimension to >10 cm class, ease of bonding with an absorber to the side for suppressing amplified spontaneous emission or parasitic lasing occurring in the radial direction, optical uniformity, and high mechanical strength. The output of laser sources may be further increased by incorporating these advantages in S-FAP. However, grain boundary scattering resulting from birefringence significantly degrades the optical transmittance of non-cubic polycrystalline ceramics, such as hexagonal S-FAP. Therefore, obtaining high optical quality in non-cubic polycrystalline ceramics is difficult. The grain

boundary scattering of non-cubic ceramics, γ, can be calculated using the following equation [5]:

$$\gamma(\lambda) = \frac{3\pi^2 d \Delta n^2}{2\lambda^2}, \quad (1)$$

where d is the average size of the grain constituting the ceramics, Δn is the average refractive index difference occurring at the grain boundaries, and λ is the wavelength of light. Non-cubic transparent ceramics can be fabricated by controlling the orientation of crystal grains to reduce Δn. In fact, laser oscillation in non-cubic ceramics such as Nd- and Yb-doped calcium fluorapatite (FAP: $Ca_{10}(PO_4)_6F_2$) was realized by controlling the crystal grain orientation using a magnetic field [6-8].

Transparent non-cubic ceramics can also be achieved by decreasing grain size d such that it is sufficiently smaller than the wavelength of light λ. This approach has been widely investigated, particularly for fabricating transparent alumina [5,9-11]. Residual pores are another main scattering source in ceramics regardless of the crystal structure of the host material; their removal generally requires high-temperature and long-term thermal treatment. In such cases, the sizes of the crystal grains tend to be in the order of several micrometers, which are larger than the wavelength of light. To achieve both full densification and nano-sized crystal grains for the realization of non-cubic transparent

ceramics, advanced ceramic fabrication technologies, including ideal nano-powder synthesis or precise sintering techniques are essential.

In a previous study, we reported laser oscillation in fine-grained non-cubic ceramics using Nd:FAP without controlling the crystal orientation [12]. Moreover, we fabricated Yb-doped FAP laser ceramics with nano-sized crystal grains of ~90 nm [13]. Although Nd- [14-16], Yb- [17-19], and Er-doped [20] transparent S-FAP ceramics have been widely reported, laser oscillation in S-FAP ceramics has not yet been achieved, to the best of our knowledge. As the emission cross-section of S-FAP is higher than that of FAP with Yb doping, a demonstration of lasing in S-FAP ceramics can enhance the potential as laser materials. Moreover, the fluorescence properties of randomly oriented ceramics in comparison with those of single crystals are rarely discussed.

In this study, transparent S-FAP ceramics doped with rare-earth elements (RE = Nd and Yb) were fabricated to realize laser oscillation. A fine powder was synthesized via liquid-phase synthesis, and spark plasma sintering (SPS) was performed to ensure full densification of the nano-sized crystal grains. The stimulated emission cross-section, an essential laser design parameter, was evaluated in terms of the fluorescence spectrum and lifetime and compared with the reported values for S-FAP single crystals. Furthermore, the laser oscillation of Nd:S-FAP ceramics was confirmed.

For the material preparation, strontium hydroxide hydrate, phosphoric acid, and RE (Nd^{3+} or Yb^{3+}) chloride hydrate were used to synthesize the initial S-FAP powders through a wet chemical route. The doping concentration of the RE was 1 at.%. Firstly, these materials were dissolved in deionized water separately. After stirring the solution, phosphoric acid aqueous solution was added dropwise to the strontium hydroxide aqueous solution over a period of approximately 1 h to synthesize a strontium hydroxyapatite ($Sr_{10}(PO_4)_6(OH)_2$) precursor. The rare earth chloride aqueous solution was typically mixed with the above resultant solution within the dropping process. Subsequently, the obtained precursor was dried and mixed with trifluoroacetamide, deionized water, and ethanol for fluorination. After drying again, it was heated to 600 °C for Nd:S-FAP and 800 °C for Yb:S-FAP. The obtained powder was sieved, followed by sintering using an SPS machine (LABOX-315, Sinter Land, Japan). A graphite mold having 10 mm inner diameter was used, and the powder was sintered in a vacuum under uniaxial pressing. The sintering temperature was monitored using a thermocouple. The sintering temperatures for Nd:S-FAP and Yb:S-FAP were 900 °C and 950 °C, respectively. The heating rate, holding time, and applied pressure were 5 °C/min, 20 min, and 80 MPa, respectively. After sintering, both ceramic surfaces were optically polished for characterization.

In the microstructure observation of the ceramics, thermal etching was performed at 800 °C for 2 h. The average grain size was evaluated from field-emission scanning electron microscopy (JSM-6701F, JEOL, Japan) images with at least 200 grains, assuming that the crystal grains were spherical [5]. The in-line transmitted spectra of the ceramics were measured using a visible-infrared spectrometer (UV-3600Plus, Shimadzu, Japan). The loss coefficient $\delta(\lambda)$, which is the sum of absorption and scattering coefficients, was estimated from the measured transmittance $T(\lambda)$, the actual thickness of the ceramics L, and refractive index dispersion $n(\lambda)$ of S-FAP [1] as $T(\lambda) = (1-R)^2\exp(-\delta(\lambda)L)$ and $R(\lambda) = (1-n(\lambda))^2/(1+n(\lambda))^2$. The in-line transmittance at 1 mm thickness was calculated for comparison.

The fluorescence spectrum and temporal time decay were measured using laser diodes (LDs) operating at 805 (for Nd:S-FAP) and 905 nm (for Yb:S-FAP). The fluorescence spectra were recorded using an optical spectrum analyzer (Q8383, Advantest, Japan). The fluorescence lifetime was calculated from a time-dependent fluorescence decay curve obtained using a photodetector.

The lasing properties of the Nd:S-FAP ceramics were examined using an experimental setup similar to that described in our previous studies [12,13]. A laser cavity, ~1 mm in length, was set using a flat dichroic mirror in conjunction with an output

coupler exhibiting a 95% reflectivity. A Nd:S-FAP ceramics sample with a thickness of 0.6 mm was used in the test. The pump source was a continuous-wave (CW) 60 W fiber-coupled LD; the core diameter of the fiber was 100 μm. Two coupling lenses of same focal length were used to focus the pump beam on the ceramic sample. The pump source operated under quasi-CW mode, with a pulse duration of 1 ms and repetition rate of 10 Hz, to mitigate potential thermal issues in the ceramics. A thermopile power meter (3A, Ophir Optronics, Israel) was utilized to measure the laser output, whereas an optical spectrum analyzer measured the corresponding spectrum.

Fig. 1(a) shows the X-ray diffraction patterns of the Nd:S-FAP and Yb:S-FAP powders and the sintered ceramics. The Nd:S-FAP and Yb:S-FAP powders were calcinated at 600 and 800 °C, respectively. The positions and intensities of the peaks in the diffraction patterns of both the powders were consistent with the standard values of S-FAP, indicating a single phase and no detectable other phases. The crystallite sizes of the powders were evaluated to be in the range of 17–30 nm for Nd:S-FAP and 25–35 nm for Yb:S-FAP powders. Moreover, the peak positions of the ceramics were similar to those of the powders. However, the relative intensities of the peaks in the diffraction patterns of the ceramics were slightly different with those of the powder. For example, the intensity of the (002) peak was lower, whereas the intensity of the (300) peak was

higher than that of the powder. This can be attributed to the pressurization effect of the powder, as discussed in previous studies [21-23]. The Lotgering-factor, which indicates the degree of crystal orientation [24], was roughly evaluated by comparing the XRD peak intensities of the ceramics with the standard values (JCPDS No. 50-1744), and the values for (h00) were 0.08 and 0.05 for Nd and Yb:S-FAP ceramics, respectively.

Fig. 1 (b) – (e) show the FE-SEM images of the powder and ceramics. The primary particles in (b) and (d) were nearly spherical or elliptical, and their sizes were <100 nm. The discrepancy in the sizes of Nd and Yb:S-FAP is ascribed to the differences in the calcination temperatures. As shown in Figs. 1(c) and (e), significantly large residual pores or secondary phases were not observed in the microstructure of the ceramics, and fine crystal grains were observed. Although a small amount of nano-sized closed pores is also discernible, as indicated by the arrow in Fig. 1(e), any optical scattering stemming from them can be considered negligible due to the pore size (~10 nm), which is significantly smaller than the lasing wavelength (~ 1 μm). The calculated average grain sizes of Nd and Yb:S-FAP were 95 and 112 nm, respectively; these values are equivalent to those of the FAP laser ceramics reported in previous studies [12,13]. Thus, these results indicate that nano-sized transparent S-FAP ceramics were successfully fabricated.

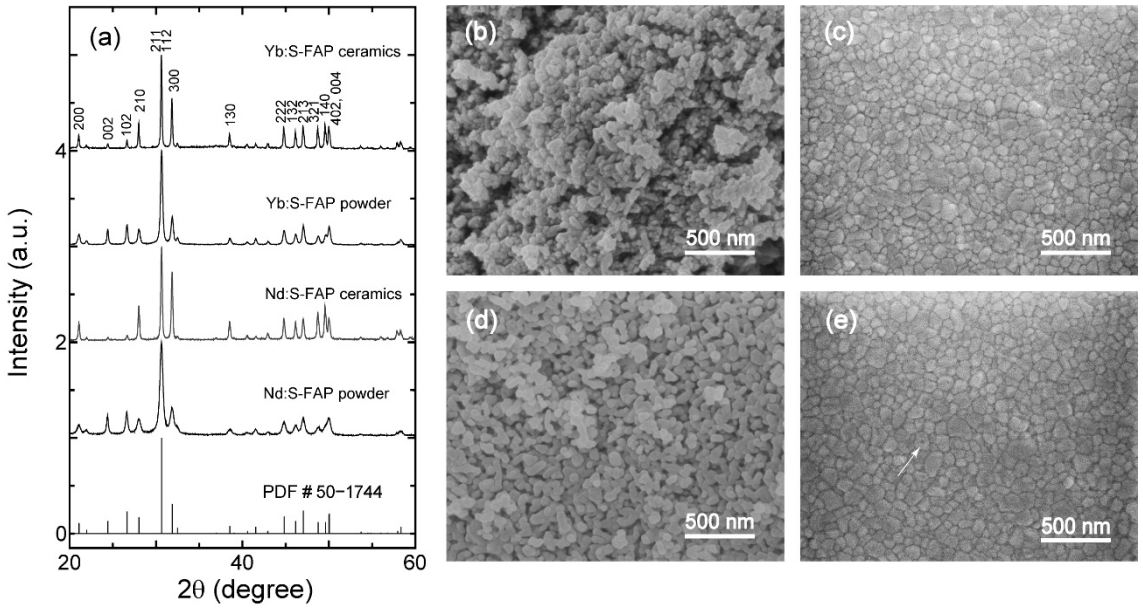

Figure 1: (a) X-ray diffraction patterns of the powders and ceramics for Nd:S-FAP and Yb:S-FAP. FE-SEM images of the (b) Nd:S-FAP powder, (c) Nd:S-FAP ceramics, (d) Yb:S-FAP powder, and (e) Yb:S-FAP ceramics. The Nd:S-FAP powder and ceramics were calcinated at 600 °C and sintered at 900 °C, whereas the Yb:S-FAP powder and ceramics were calcinated at 800 °C and sintered at 950 °C.

Figs. 2(a) and (b) show the in-line transmitted spectra of the Nd and Yb:S-FAP ceramics, respectively. The insets show the photographs of each sample, and they exhibited high transparency. For Nd:S-FAP, the in-line transmittance at the predicted laser wavelength of 1060 nm was 85.6%, and the corresponding loss coefficient calculated from the theoretical transmittance was 0.42 cm^{-1}. In addition, at 1328 nm, which is another emitting wavelength of Nd:S-FAP as described below, the in-line transmittance and loss coefficient were 86.6% and 0.30 cm^{-1}, respectively. The scattering

coefficient at longer wavelengths can be decreased because the scattering due to grain boundaries depends on the wavelength of light, as shown in Eq. (1). Thus, we can also expect efficient laser operation of Nd:S-FAP ceramics in the 1300 nm wavelength range.

For the Yb:S-FAP ceramics, the transmittance and loss coefficients at a wavelength of 1047 nm were 85.5% and 0.43 cm^{-1}, respectively. These values were almost the same values with those for Nd:S-FAP at 1060 nm, despite re-absorption loss in Yb-doped materials at the emitting wavelength at room temperature. The fabrication processes of Nd:S-FAP and Yb:S-FAP ceramics differ primarily in terms of the heat treatment conditions; thus, a higher optical quality may be obtained by optimizing the calcination and sintering temperatures.

Figs. 2(c) and (d) show the loss coefficient, which is the sum of absorption and scattering coefficients, of the Nd:S-FAP and Yb:S-FAP ceramics, respectively. For Nd:S-FAP, strong absorption peaks were observed at 793, 805, 855, and 882 nm, which correspond well with those of the Nd:S-FAP single crystals [25]. These results confirm that the Nd^{3+} ion can be substituted with the Sr site in the S-FAP structure. For Yb:S-FAP, strong absorption peaks at 900, 977, and 985 nm were observed (Fig. 2(d)); however, typical Yb:S-FAP single crystals show strong peaks at only 900 and 985 nm [26]. The anomalous absorption peak and the absorption band at 977and 925–1000 nm could be

ascribed to the Yb^{3+} ions incorporation at a secondary site (Sr_{II}) in the crystal lattice, as detailed in a previous study [1]. The anomalous peak might also be attributed to the precipitation of an extremely small amounts of other phases, such as Yb_2O_3 or Yb-doped tri-strontium phosphate ($Sr_3(PO_4)_2$) that were not detected by XRD measurements. These interferences are factors that prevent efficient excitation; therefore, they must be reduced to obtain sufficient emission from Yb:S-FAP for laser oscillation. To this end, several approaches are being investigated.

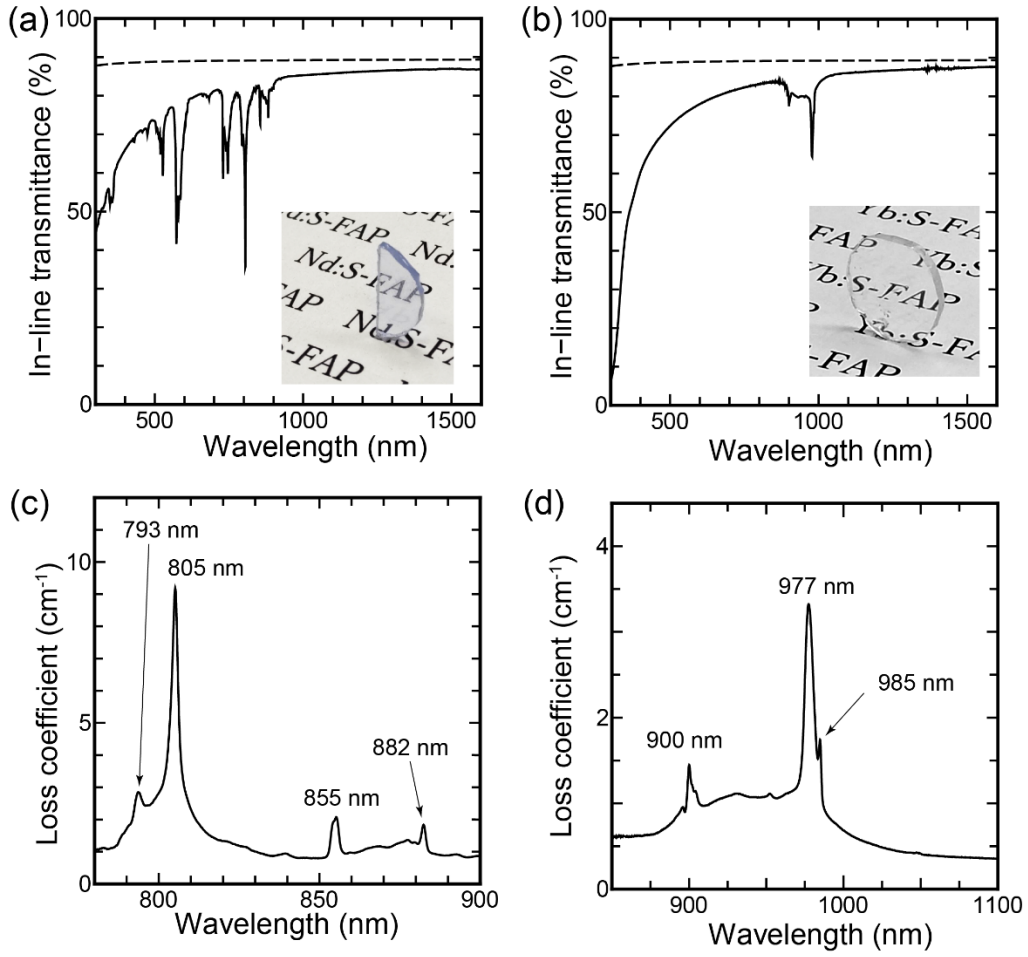

Figure 2: In-line transmitted spectra of the (a) Nd:S-FAP and (b) Yb:S-FAP ceramics. The insets show the photographs of the ceramics. Corresponding loss coefficient of the (c) Nd and (d) Yb:S-FAP ceramics.

Figs. 3(a) and (b) show the fluorescence decay curves of Nd:S-FAP and Yb:S-FAP, respectively. The curve for the Nd:S-FAP ceramics fitted well with a double exponential function: $I(t) = A_1 \exp(-t/\tau_1) + A_2 \exp(-t/\tau_2)$. The average lifetime of the Nd:S-FAP ceramics was calculated using the following relation [27]:

$$\tau = \left(A_1\tau_1^2 + A_2\tau_2^2\right) \Big/ \left(A_1\tau_1 + A_2\tau_2\right) \quad (2)$$

The lifetime of Yb:S-FAP was fitted with a single exponential curve: $I(t) = A\exp(-t/\tau)$. The calculated lifetimes of Nd and Yb:S-FAP were 229 μs and 1.0 ms, respectively. The fluorescence properties of Nd:S-FAP and Yb:S-FAP are summarized in Table 1 and 2, respectively; the values reported for the single crystals are also shown for comparison. The differences between the lifetimes of single crystals and ceramics were not significant.

The stimulated emission cross-sections of the S-FAP ceramics were evaluated using the well-known Füchtbauer–Ladenburg (FL) equation [31]. Figs. 3(c) and (d) show the stimulated emission cross-section σ_e of the Nd:S-FAP and Yb:S-FAP ceramics, respectively. The wavelengths of the emission peaks of the Nd:S-FAP and Yb:S-FAP ceramics were similar to those of the single crystals. The Nd:S-FAP ceramics exhibited emission peaks at 1059 and 1328 nm with emission cross-section of 2.0×10^{-19} and 7.3×10^{-20} cm^2, respectively. Also, the Yb:S-FAP ceramics exhibited emission peaks at 985 and 1047 nm with emission cross-section of 7.1×10^{-20} and 3.6×10^{-20} cm^2, respectively.

A comparison of the emission cross-section indicates that the highest σ_e values of the ceramics were smaller than those of single crystals. This is attributed to the anisotropic characteristics of non-cubic crystals. As shown in Table 2, the σ_e values of Yb:S-FAP single crystal at 1047 nm for both the P (E // c) and S (E $\perp$ c) polarization were different,

and the values for P polarization were higher. In contrast, the ceramics are composed of randomly oriented multiple crystal grains, the σ_e value of the ceramics is between the values of each polarization for a single crystal. Assuming that the average emission cross-section of the ceramics is given by

$$\sigma_{av} = \left(\sigma(P) + 2\sigma(S)\right)/3, \quad (3)$$

the calculated σ_{av} values for the Yb:S-FAP were 8.3×10^{-20} and 3.5×10^{-20} cm^2 at 985 and 1047 nm, which are in reasonably agreement with the experimental results. As shown in Fig. 1, the orientation of the grains in the ceramics studied in this work is not completely random; hence, detailed analyses are necessary. Nevertheless, we believe that this finding is important for the design and development of next-generation non-cubic ceramics as efficient laser materials.

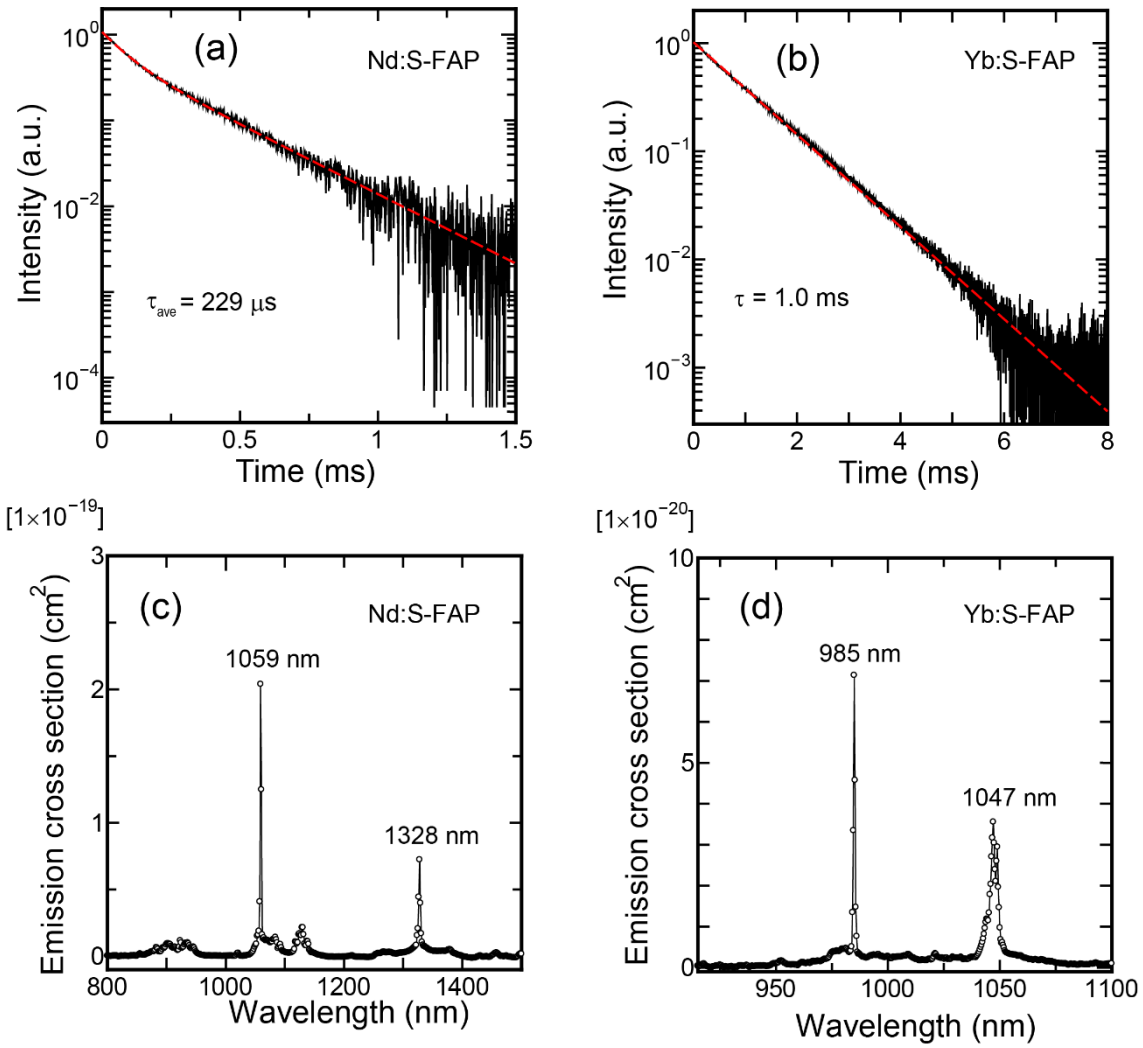

Figure 3: Fluorescence time decay of the (a) Nd:S-FAP and (b) Yb:S-FAP ceramics. Emission spectra of the (c) Nd:S-FAP and (d) Yb:S-FAP ceramics.

Table 1. Fluorescence properties of the Nd:S-FAP single crystal and ceramics. Here, λ denotes the wavelength of light, σ_e is the emission cross-section, and τ is the lifetime.

Host material	λ (nm)	σ_e × 10^{-19} (cm^2)	τ (μs)	Refs.
Nd:S-FAP single crystal	1059	5.4	190	[28]
	1328	2.3		
Nd:S-FAP single crystal	1059	6.4	290	[29]
Nd:S-FAP Ceramics	1059	2.0	229	This work
	1328	0.7		

Table 2. Fluorescence properties of the Yb:S-FAP single crystal and ceramics.

Host material	λ (nm)	σ_e × 10^{-20} (cm^2)	τ (ms)	Refs.
Yb:S-FAP single crystal	1047	6.0 (E ∥ c)	1.14	[1]
Yb:S-FAP single crystal	985	4.9 (E ∥ c) 10 (E ⊥ c)	1.26	[26]
	1047	7.3 (E ∥ c) 1.6 (E ⊥ c)		
Yb:S-FAP single crystal	985	10 (E ⊥ c)	1.14	[30]
Yb:S-FAP Ceramics	985	7.1	1.0	This work
	1047	3.6		

The laser output characteristics of the Nd:S-FAP ceramics are shown in Fig. 4. The inset shows the lasing spectrum oscillating at 1058 nm. The slope efficiency was 6.3% with respect to the absorbed pump power. As well in the previous study [12], higher output power and efficiency can be expected by introducing a cooling system, depositing an anti-reflection coating, and utilizing a more suitable cavity configuration.

To the best of our knowledge, this is the first study on laser oscillation in S-FAP ceramics. Although laser oscillation has not been observed in the Yb:S-FAP ceramics in this study, it can possibly be realized by using an ideal pump source. The major reason is that the wavelength of the pump LD used for the lasing test was 905 nm under QCW operation and did not match well with the absorption peak of Yb:S-FAP as shown in Fig. 2(d). In addition, as the maximum output peak power of the LD was 30 W, a more powerful pump source was available. Moreover, we intend to optimize the fabrication process of Yb:S-FAP to increase the absorption at a wavelength of 900 nm by reduction the anomalous absorption. We believe that the application scope of non-cubic ceramics as laser materials can be further expanded by improving the optical quality, increasing the size, and controlling the orientation of the crystals.

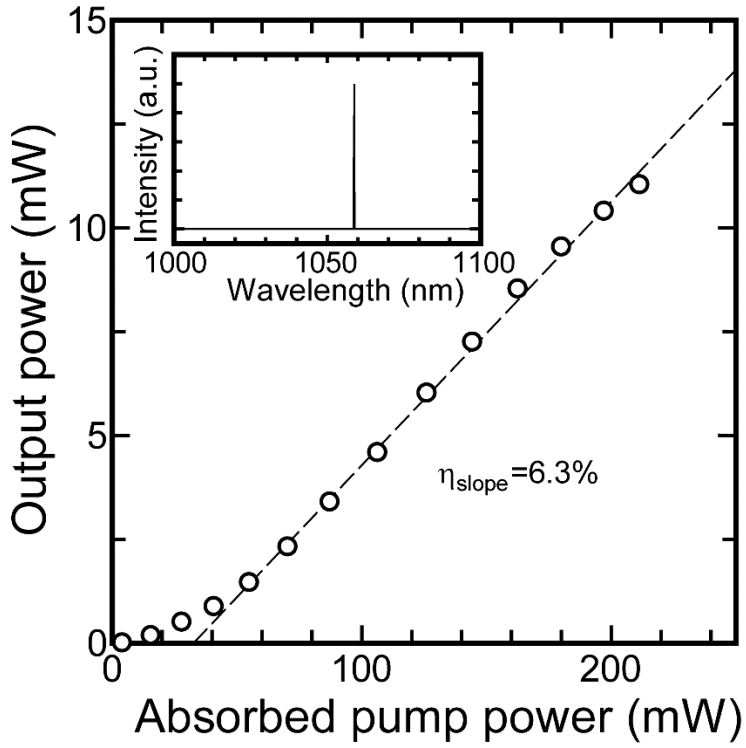

Figure 4: Laser output power as a function of the absorbed pump power. The inset shows the lasing spectrum.

Conflict of Interest

All authors declare no conflicts of interests.

Funding

This work was supported by JST FOREST Program (Grant Number JPMJFR203S) and JSPS KAKENHI (Grant Number 21H01611).

References

[1] K.I. Schaffers, J.B. Tassano, A.B. Bayramian, R.C. Morris, Growth of Yb: S-FAP [Yb^{3+}:$Sr_5(PO_4)_3F$] crystals for the Mercury laser, J. Cryst. Growth. 253 (2003) 297–306. https://doi.org/10.1016/S0022-0248(03)01032-7.

[2] A.C. Erlandson, S.M. Aceves, A.J. Bayramian, A.L. Bullington, R.J. Beach, C.D. Boley, J.A. Caird, R.J. Deri, A.M. Dunne, D.L. Flowers, M.A. Henesian, K.R. Manes, E.I. Moses, S.I. Rana, K.I. Schaffers, M.L. Spaeth, C.J. Stolz, S.J. Telford, Comparison of Nd:phosphate glass, Yb:YAG and Yb:S-FAP laser beamlines for laser inertial fusion energy (LIFE), Opt. Mater. Express 1 (2011) 1341–1352. https://doi.org/10.1364/OME.1.001341.

[3] P. Mason, M. Divoký, K. Ertel, J. Pilař, T. Butcher, M. Hanuš, S. Banerjee, J. Phillips, J. Smith, M. De Vido, A. Lucianetti, C. Hernandez-Gomez, C. Edwards, T. Mocek, J. Collier, Kilowatt average power 100 J-level diode pumped solid state laser, Optica 4 (2017) 438–439. https://doi.org/10.1364/OPTICA.4.000438.

[4] M. Divoký, J. Pilař, M. Hanuš, P. Navrátil, O. Denk, P. Severová, P. Mason, T. Butcher, S. Banerjee, M. De Vido, C. Edwards, J. Collier, M. Smrž, T. Mocek, 150 J DPSSL operating at 1.5 kW level, Opt. Lett. 46 (2021) 5771–5773. https://doi.org/10.1364/OL.444902.

[5] R. Apetz, M.P.B. Van Bruggen, Transparent alumina: A light-scattering model, J. Am. Ceram. Soc. 86 (2003) 480–486. https://doi.org/10.1111/j.1151-2916.2003.tb03325.x.

[6] J. Akiyama, Y. Sato, T. Taira, Laser ceramics with rare-earth-doped anisotropic materials, Opt. Lett. 35 (2010) 3598–3600. https://doi.org/10.1364/OL.35.003598.

[7] J. Akiyama, Y. Sato, T. Taira, Laser demonstration of diode-pumped Nd^{3+}-doped fluorapatite anisotropic ceramics, Appl. Phys. Express 4 (2011) 022703. https://doi.org/10.1143/APEX.4.022703.

[8] Y. Sato, J. Akiyama, T. Taira, Process design of microdomains with quantum mechanics for giant pulse lasers, Sci. Rep. 7 (2017) 10732. https://doi.org/10.1038/s41598-017-10884-z.

[9] B.N. Kim, K. Hiraga, K. Morita, H. Yoshida, Spark plasma sintering of transparent alumina, Scr. Mater. 57 (2007) 607–610. https://doi.org/10.1016/j.scriptamat.2007.06.009.

[10] B. Ratzker, A. Wagner, B. Favelukis, I. Ayalon, R. Shrem, S. Kalabukhov, N. Frage, Effect of synthesis route on optical properties of Cr:Al_2O_3 transparent ceramics sintered under high pressure, J. Alloys Compd. 913 (2022) 165186. https://doi.org/10.1016/j.jallcom.2022.165186.

[11] E.H. Penilla, L.F. Devia-Cruz, M.A. Duarte, C.L. Hardin, Y. Kodera, J.E. Garay, Gain in polycrystalline Nd-doped alumina: Leveraging length scales to create a new class of high-energy, short pulse, tunable laser materials, Light Sci. Appl. 7 (2018) 33. https://doi.org/10.1038/s41377-018-0023-z.

[12] H. Furuse, N. Horiuchi, B.N. Kim, Transparent non-cubic laser ceramics with fine microstructure, Sci. Rep. 9 (2019) 10300. https://doi.org/10.1038/s41598-019-46616-8.

[13] H. Furuse, T. Okabe, H. Shirato, D. Kato, N. Horiuchi, K. Morita, B.-N. Kim, High-optical-quality non-cubic Yb^{3+}-doped $Ca_{10}(PO_4)_6F_2$ (Yb:FAP) laser ceramics, Opt. Mater. Exp. 11 (2021) 1756–1762. https://doi.org/10.1364/OME.426701.

[14] Y. Zhang, B. Mei, W. Li, Y. Yang, G. Yi, Z. Zhou, Z. Liu, Fabrication and spectral properties of Nd:S-FAP transparent ceramics by simple route of HP method, J. Alloys Compd. 820 (2020) 153171. https://doi.org/10.1016/j.jallcom.2019.153171.

[15] Y. Zhang, Z. Zhou, W. Li, Y. Yang, B. Mei, Z. Sun, The effect of Nd^{3+} concentration on fabrication, microstructure, and luminescent properties of anisotropic S-FAP ceramics, J. Am. Ceram. Soc. 105 (2022) 2932–2944. https://doi.org/10.1111/jace.18284.

[16] Y. Zhang, Z. Zhou, B. Mei, Y. Yang, The effect of Y^{3+} doping upon Nd: S-FAP transparent ceramics for effective spectral performance improvement, Ceram. Int. 49 (2023) 1362–1368. https://doi.org/10.1016/j.ceramint.2022.09.117.

[17] S. Chen, Y. Wu, Y. Yang, Spark plasma sintering of hexagonal structure Yb^{3+}-doped $Sr_5(PO_4)_3F$ transparent ceramics, J. Am. Ceram. Soc. 96 (2013) 1694–1697. https://doi.org/10.1111/jace.12362.

[18] X. Liu, G. Tan, W. Li, B. Mei, Conventional HP sintering of asymmetric hexagonal structure Yb^{3+}-doped $Sr_5(PO_4)_3F$ transparent ceramic without additives, J. Am. Ceram. Soc. 105 (2022) 4581–4587. https://doi.org/10.1111/jace.18451.

[19] X. Liu, G. Tan, Z. Zhou, B. Mei, Fabrication, microstructure, mechanical and luminescence properties of transparent Yb^{3+}-doped $Sr_5(PO_4)_3F$ nanostructured ceramics, J. Eur. Ceram. Soc. 42 (2022) 6642–6653. https://doi.org/10.1016/j.jeurceramsoc.2022.07.041.

[20] D. Permin, M. Nazmutdinov, S. Kurashkin, S. Balabanov, A. Belyaev, A. Novikova, V. Koshkin, Fabrication and luminescent properties of Er-doped $Sr_5(PO_4)_3F$ ceramics, Inorganics 11 (2023) 57. https://doi.org/10.3390/inorganics11020057.

[21] Y. Watanabe, T. Ikoma, A. Monkawa, Y. Suetsugu, H. Yamada, J. Tanaka, Y. Moriyoshi, Fabrication of transparent hydroxyapatite sintered body with high crystal

orientation by pulse electric current sintering, J. Am. Ceram. Soc. 88 (2005) 243-245. https://doi.org/10.1111/j.1551-2916.2004.00041.x.

[22] Z. Li, B.C. Thompson, Z. Dong, K.A. Khor, Optical and biological properties of transparent nanocrystalline hydroxyapatite obtained through spark plasma sintering, Mater. Sci. Eng. C 69 (2016) 956-966. https://doi.org/10.1016/j.msec.2016.08.002.

[23] H. Furuse, D. Kato, K. Morita, T.S. Suzuki, B.N. Kim, Characterization of transparent fluorapatite ceramics fabricated by spark plasma sintering, Materials 15 (2022) 8157. https://doi.org/10.3390/ma15228157.

[24] F.K. Lotgering, Topotactical reactions with ferrimagnetic oxides having hexagonal crystal structures – I, J. Inorg. Nucl. Chem. 9 (1959) 113–123. https://doi.org/10.1016/0022-1902(59)80070-1

[25] J.B. Gruber, C.A. Morrison, M.D. Seltzer, A.O. Wright, M.P. Nadler, T.H. Allik, J.A. Hutchinson, B.H.T. Chai, Site-selective excitation and polarized absorption spectra of Nd^{3+} in $Sr_5(PO_4)_3F$ and $Ca_5(PO_4)_3F$, J. Appl. Phys. 79 (1996) 1746–1758. https://doi.org/10.1063/1.360964.

[26] L.D. DeLoach, S.A. Payne, L.K. Smith, W.L. Kway, W.F. Krupke, Laser and spectroscopic properties of $Sr_5(PO_4)_3F$:Yb, J. Opt. Soc. Am. B 11 (1994) 269–276. https://doi.org/10.1364/JOSAB.11.000269.

[27] A. Sillen, Y. Engelborghs, The correct use of “average” fluorescence parameters, Photochem. Photobiol. 67 (1998) 475–486. https://doi.org/10.1111/j.1751-1097.1998.tb09082.x.

[28] X.X. Zhang, P. Hong, G.B. Loutts, J. Lefaucheur, M. Bass, B.H.T. Chai, Efficient laser performance of Nd^{3+}:$Sr_5(PO_4)_3F$ at 1.059 and 1.328 μm, Appl. Phys. Lett. 64 (1994) 3205–3207. https://doi.org/10.1063/1.111337.

[29] X. Zhang, S. Zhao, Q. Wang, L. Sun, S. Zhang, G. Yao, Z. Zhang, Laser diode pumped Cr^{4+}:YAG passively Q-switched Nd^{3+}:S-FAP laser, Opt. Commun. 155 (1998) 55–60. https://doi.org/10.1016/S0030-4018(98)00356-3

[30] S. Yiou, F. Balembois, K. Schaffers, P. Georges, Efficient laser operation of an Yb:S-FAP crystal at 985 nm, Appl. Opt. 42 (2003) 4883–4886. https://doi.org/10.1364/ao.42.004883.

[31] W.F. Krupke, M.D. Shinn, J.E. Marion, J.A. Caird, S.E. Stokowski, Spectroscopic, optical, and thermomechanical properties of neodymium-and chromium-doped gadolinium scandium gallium garnet, J. Opt. Soc. Am. B 3 (1986) 102–114. https://doi.org/10.1364/JOSAB.3.000102.